Topology and transport in the edge region of RFX-mod helical regimes

2011 Nucl. Fusion 51 073002

(http://iopscience.iop.org/0029-5515/51/7/073002)

IOP Publishing and International Atomic Energy Agency Nuclear Fusion
Nucl. Fusion **51** (2011) 073002 (11pp) doi:10.1088/0029-5515/51/7/073002

Topology and transport in the edge region of RFX-mod helical regimes

P. Scarin, N. Vianello, M. Agostini, G. Spizzo, M. Spolaore, M. Zuin, S. Cappello, L. Carraro, R. Cavazzana, G. De Masi, E. Martines, M. Moresco, S. Munaretto, M. E. Puiatti, M. Valisa and the RFX-mod Team

Consorzio RFX, Associazione Euratom-ENEA sulla fusione, C.so Stati Uniti 4, I-35127 Padova, Italy

E-mail: paolo.scarin@igi.cnr.it and nicola.vianello@igi.cnr.it

Received 23 December 2010, accepted for publication 20 April 2011
Published 25 May 2011
Online at stacks.iop.org/NF/51/073002

Abstract
New edge diagnostics and detailed analysis of magnetic topology have significantly improved the comprehension of the processes developing at the boundary of a reversed-field pinch (RFP) plasma in RFX-mod ($a = 0.46$ m, $R = 2$ m).

An upper critical density $n_C \approx 0.4\, n_G$ (n_G Greenwald density) is found to limit the operational space for the improved quasi-single helical (QSH) regime: magnetic topology reconstructions and diagnostic observations suggest that this limit is due to a helical plasma–wall interaction which determines toroidally and poloidally localized edge density accumulation and cooling.

The experimental evidence is provided by a variety of diagnostics: the magnetic boundary as reconstructed from equilibrium codes reveals a helical deformation, which is well correlated with the modulation of edge pressure profile as reconstructed from the thermal helium beam diagnostic. Correlations with the helical deformation are also observed on the space- and time-resolved patterns of the floating potential measured at the wall, and with the edge plasma flow, obtained from different diagnostics. The relevance of these findings is that understanding the mechanisms that limit the operational space of QSH is decisive in achieving the goal of high-density stationary helical RFP equilibrium.

(Some figures in this article are in colour only in the electronic version)

1. Introduction

The reversed-field pinch (RFP) RFX-mod device ($a = 0.46$ m, $R = 2$ m) exploits a toroidal configuration for plasma confinement with the safety factor profile q monotonically decreasing from the core to the edge, where it changes sign. The amelioration of the plasma boundary control through the feedback system of active coils [1–4] and the increase in plasma current revealed a spontaneous transition from the chaotic multiple helical (MH) state, characterized by a broad spectrum of internally resonating MHD modes, to the quasi-single helical (QSH) regime. QSH shows an almost monochromatic MHD spectrum induced by the increase of the dominant ($m = 1, n = -7$) mode, which is the innermost resonating one, and the simultaneous decrease of the secondary modes with $m = 1$ and $|n| > 7$, leading to an improved magnetic topology with good magnetic flux surfaces [5]. When the amplitude of the dominant mode exceeds a critical value, the QSH spontaneously bifurcates, the separatrix is expelled and the system evolves towards a helical equilibrium, dubbed single helical axis or SHAx state, associated with an internal electron transport barrier [6, 7]. QSH transitions are most easily encountered at shallow reversal [8] ($q(a) = -0.015$ to -0.0015) where empirical evidence of reduced plasma–wall interaction (PWI) is observed [9], whereas deeper reversal equilibria exhibit a more severe PWI caused also by wall locking of MHD modes. As predicted by the non-linear visco-resistive MHD code Specyl [10], shallow reversal equilibria are characterized by a systematically lower amplitude of $m = 0$ modes [11]. Currently, QSH states are not stationary: although they may last tens of energy confinement times, they undergo fast interruptions (crashes) linked to magnetic reconnection events [6, 7]. Crucial to the assessment of the RFP as a viable configuration for plasma confinement are therefore the explanation of the non-stationarity of the QSH state, the widening of its operational space and the amelioration of the PWI, which contributes to the power input (~30 MW), still large even in the QSH state [6, 7].

Equilibrium reconstructions reveal that despite the fact that the boundary surrounding the helical core in QSH-SHAx is quasi-symmetric [12] and the contribution of the edge helical ripple to neoclassical transport is negligible [13], the residual ripple at the edge can have an impact on transport parallel to the field. This paper focuses on the effects of this helical topology on the properties of the edge plasma. Indeed, it will be shown how the helical deformation induced by the dominant mode $(1, -7)$, described by the radial plasma shift $\Delta_{1,-7}$, modulates edge quantities such as electron pressure P_e, floating potential V_f or H_α emission. The edge plasma topology is further complicated by the presence of the $q = 0$ surface dubbed reversal surface and the corresponding spectrum of $m = 0$ modes. Indeed, the reversal surface hosts a chain of poloidally symmetric $m = 0$ islands which are numerically proved to strongly influence particle diffusivity at the edge [14]. In particular, while ion diffusion is found to be similar in O- and X-points of the $(0, 7)$ islands, electrons are observed to spend more time in X-points due to their smaller drifts. The result is a toroidal modulation of the electron diffusion with an $n = 7$ pattern and a corresponding toroidal modulation of radial ambipolar electric field which builds up to ensure plasma quasi-neutrality [15]. Experimental evidence of the toroidal modulation of the toroidal flow (which, neglecting diamagnetic contribution, may be directly linked to the radial electric field) will be provided in the text.

The second part of the paper will be focused on QSH dynamics and in particular on the back transition from QSH to MH states, coupled to spontaneous reconnection events. These crash events limit the QSH persistence and the possibility to prolong improved confinement regimes. The paper will provide experimental evidence of the increase in crash frequency with the normalized plasma density n_e/n_G and also with relatively lower $q(a)$ values. Both these experimental conditions involve the increase in the $m = 0$ mode amplitude and in the associated PWI [15].

This paper is organized as follows: section 2 provides a description of the plasma boundary topology and its relationship with edge quantities, namely particle fluxes, electron pressure, floating potential and plasma flow. Section 3 is focused on the QSH persistence and QSH–MH back transition, plus some considerations on magnetic reconnection. Section 4 is dedicated to the discussion of the critical density limiting the operational space where QSH can develop, and in section 5 we draw our conclusions.

2. Plasma boundary description

2.1. Magnetic structure and PWI

The edge region of RFX-mod is characterized by the presence of a chain of $(0, 7)$ islands arising because of the resonances of $m = 0$ modes and/or the beating of $m = 1$ ones [9, 14]. The radial width of the islands is $\sim$10 cm at 0.8 MA and $\sim$14 cm at 1.5 MA, and it is comparable in both QSH and MH states only at a low current [15]. Nevertheless, while in the QSH state the edge topology is uniform, with the island X- and O-points aligned along the reversal surface, in the MH state the edge topology is toroidally asymmetric. The asymmetry is determined by the presence of an $(m, n) = (0, 1)$ mode arising as a consequence of the phase locking of various $m = 1$ modes.

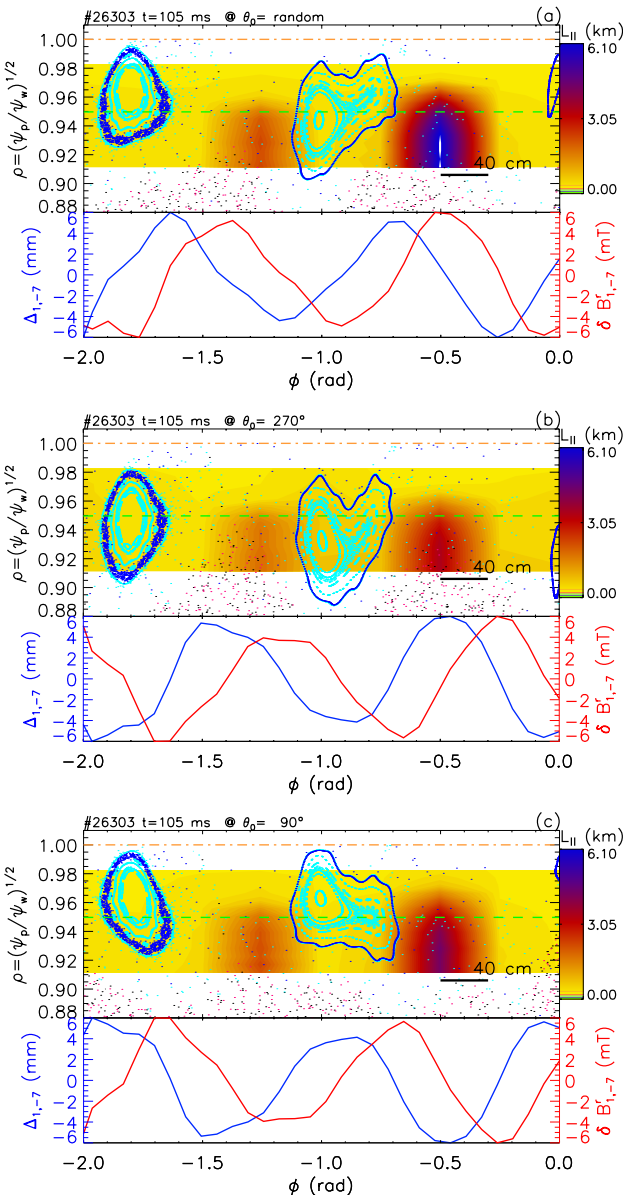

Figure 1. (a) Top: Poincaré plot as obtained from the ORBIT code, equatorial cut at $\theta = 0$. Colour codes indicate the electron characteristic length $L_\parallel$ defined as the length of the path followed by the electrons parallel to the magnetic field from their initial position $(\rho_0, \theta_0, \phi_0) = (0.99, \text{random}, \phi_0)$ to their exit position $(\rho_1, \theta_1, \phi_1) = (\rho_1, \text{random}, \text{random})$. The map describes $L_\parallel(\rho_1, \theta_0, \phi_0)$. (a) Bottom: horizontal shift of the dominant mode $\Delta_{1,-7}$ (blue line), radial magnetic field perturbation of the dominant mode (red line). (b), (c) The same as in (a), but initializing particles at $\theta_0 = 270°$ and $\theta_0 = 90°$, respectively. The Poincaré cut is performed at the same angle, $\theta = 270°$ and $\theta = 90°$: in other words, (b) represents the bottom and (c) the top of the machine.

A zoom of a Poincaré plot at poloidal angle $\theta = 0°$, obtained with the Hamiltonian guiding centre, single-particle code ORBIT [16], is shown in figure 1(a), top panel, simulating a QSH plasma discharge at $I_p = 0.8$ MA, $q(a) = -0.01$ and $n_e/n_G = 0.2$, and highlighting the $(0, 7)$ island pattern. This $m = 0$ topology, which is symmetric in the poloidal angle θ and depends only on the toroidal angle ϕ, is further complicated by the non-linear interaction with the $m = 1, n = -7$ mode [9].

In the rest of this paper we will characterize this θ-modulation by comparing the Poincaré plot of $m = 0$ islands with the shape of the $m = 1$ plasma radial shift, $\Delta_{1,-7}$. This shift is evaluated at $r = a$ and is a function of both poloidal and toroidal angles, $\Delta_{1,-7} = \Delta_{1,-7}(\theta, \phi)$ [17]. We will use $\Delta_{1,-7}$ as a proxy of the phase relationship between $m = 0$ and $m = 1$ modes, since the maximum $\Delta_{1,-7}$ corresponds to the O-point of the dominant $m = 1$ mode, thus describing the global helical shaping of the plasma column. Toroidally, this means that $\frac{\partial \Delta_{1,-7}}{\partial \phi} = 0$ at the O-point of the $(1, -7)$ mode.

The colour code in figure 1(a) refers to the contour map of the parallel electron characteristic length, defined as $L_\parallel(r, \theta, \phi) \simeq v_{\rm th}\tau_{\rm trav}$, where $v_{\rm th}$ is the electron thermal velocity, and $\tau_{\rm trav}$ is the electron travel time between an initial $(\rho_0, \theta_0, \phi_0)$ and final position $(\rho_1, \theta_1, \phi_1)$. $L_\parallel$ in other words represents the length of the path followed by the electron guiding centres in the direction parallel to the field, when travelling from some prescribed positions to the recovery surface. In figure 1(a) we define the initial and final conditions as $(\rho_0, \theta_0, \phi_0) = (0.99,\ \text{random},\ \phi_0)$ and $(\rho_1, \theta_1, \phi_1) = (\rho_1,\ \text{random},\ \text{random})$, respectively. We imposed a simple model of a recycling wall in the simulations, as done in [15]. Electrons are thermal, with temperature $T_{\rm e} \sim 270$ eV. Collisions happen with ions, electrons, and C^{4+} and O^{6+} impurities, with background edge temperature $T_{\rm b} = 20$ eV and density $n_{\rm b} = 4 \times 10^{19}\,{\rm m}^{-3}$. The definition of $L_\parallel$ is such that each individual volume element in the map represents the length the electron travelled to arrive at ρ_1, starting from $(\rho_0, \theta_0, \phi_0)$, namely $L_\parallel = L_\parallel(\rho_1, \theta_0, \phi_0)$, similarly to what was done in [9]. Obviously, this length depends on the initial conditions, but the problem is not completely solved even if one defines averages on the final and/or initial positions (average over 1000 particles in our simulations), since the magnetic field is weakly chaotic in the RFX-mod edge. The only mathematically well-defined observable is the Poincaré recurrence time, which is a property of only the volume [18]. Efforts in this direction are ongoing. Even with this loose definition, the length $L_\parallel$ exhibits a modulation of more than one order of magnitude moving from X-points to O-points of the $(0, 7)$ islands, with electrons sticking in the vicinity of X-points, and moving in and out freely near O-points. In the bottom panel of figure 1(a) the radial shift of the dominant mode $\Delta_{1,-7}(\phi)$ and the corresponding radial magnetic field perturbation $\delta B^r_{1,-7}(\phi)$ are also shown as a function of the toroidal angle ϕ for a fixed time and at $\theta = 0^\circ$. The maximum radial shift of the $(1, -7)$ mode is between the O- and X-points of the $(0, 7)$ islands, whereas the maximum radial magnetic field corresponds to the X-points.

As pointed out at the beginning of this section, this relation has a poloidal angle dependence due to the phase relation between the $(1, -7)$ mode and its $m = 0$ counterpart. In fact, figure 1(b) shows the same plots as in panel (a), but performing the Poincaré cut at $\theta = 270^\circ$ and initializing particles at $(\rho_0, \theta_0, \phi_0) = (0.99, 270^\circ, \phi_0)$, i.e. with θ_0 the same as the Poincaré cut, instead of random. Comparing the top and bottom panels in figure 1(b), one sees that the maximum $\Delta_{1,-7}(\phi)$ corresponds to the X-points of the $(0, 7)$ islands. The contour map of $L_\parallel$ (top panel) shows a toroidal spatial pattern similar to figure 1(a), but with a maximum of $\sim$3 km, approximately half of the random θ_0 case. We repeated

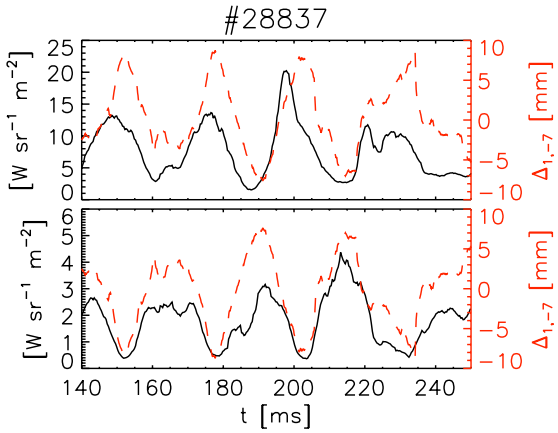

Figure 2. H_α emission (black) compared with local magnetic shift induced by the dominant mode (red) in the LFS (top) and HFS (bottom).

the exercise by performing the Poincaré cut at $\theta = 90^\circ$ and initializing particles for the $L_\parallel$ calculations at $\theta_0 = 90^\circ$, as shown in figure 1(c). Comparing the top and bottom panels, now the maximum $\Delta_{1,-7}(\phi)$ corresponds to the O-points of the (0,7) islands, i.e. O-points of $m = 1$ and $m = 0$ islands are aligned along ϕ, and the same for X-points (we remind the reader that the maximum $\Delta_{1,-7}$ corresponds to the position of the O-point of the $(1, -7)$ island). The contour map of $L_\parallel$ (top panel) shows a toroidal spatial pattern similar to figures 1(a) and (b), but with a maximum of $\sim$4 km. Comparing $L_\parallel$ at $\theta = 90^\circ$ and 270°, we see that the larger value is found at 90° (top of the machine), since the parallel length near the $m = 0$ X-point sums up non-linearly to the $m = 1$ contribution. The opposite happens at $\theta = 270^\circ$, where the $m = 0$ X-point contribution sums up to the $m = 1$ O-point contribution. In both cases, anyway, $L_\parallel$ is below average (initial θ_0 random, see figure 1(a)), meaning that the maximum $L_\parallel$ will be found at another poloidal position.

Particle behaviour is strongly influenced by the peculiar magnetic topology observed at the edge: qualitatively the dynamics around the O- and X-points of $(0, 7)$ islands in QSH resembles the previously documented behaviour observed around the $(0, 1)$ island in MH [15]. Indeed in MH states the maximum radial shift corresponding to the secondary modes with $m = 1$ and $|n| > 7$ is located between the O- and X-points of the $(0, 1)$ island and constitutes the main particle source [19]. In QSH the particle source is toroidally distributed and modulated by the $\Delta_{1,-7}$ shift, exhibiting, in the equatorial plane, seven maxima between the O- and X-points of the $(0, 7)$ islands. This can be seen in figure 2 where signals of H_α emission along two vertical chords (low- (LFS) and high-field side (HFS) at the same toroidal position) are compared with the magnetic shifts as reconstructed from edge magnetic measurements at the proper toroidal and poloidal positions [17]. In both positions H_α maxima are observed for positive values of the $\Delta_{1,-7}$ shift and the two chords are anti-correlated indicating an $m = 1$ symmetry, namely a helical pattern of PWI. The different H_α emissivity values at the HFS and LFS are caused by an in–out asymmetry of the helical structure due to the Shafranov shift of the magnetic axis, which can be of the order of a few centimetres: the same helical flux surface is closer to the wall in the LFS than in the HFS [12].

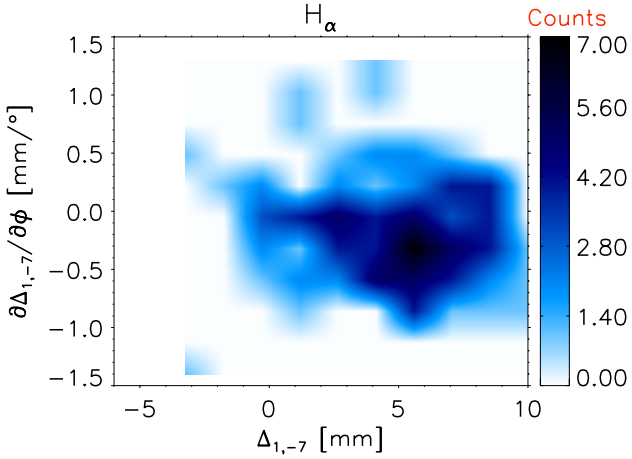

Figure 3. 2D PDF of H_α maxima as a function of $\Delta_{1,-7}$ and $\frac{\partial\Delta_{1,-7}}{\partial\phi}$.

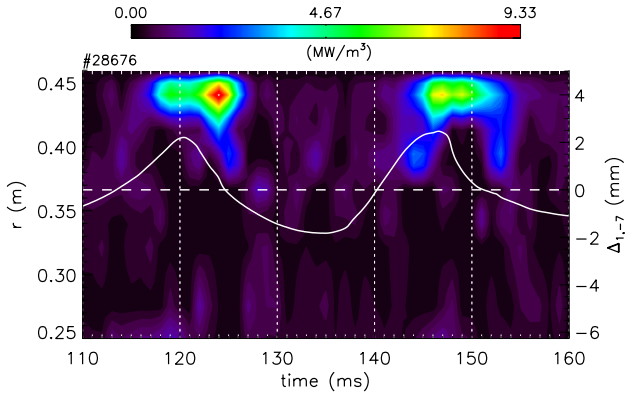

Figure 4. Total radiation emissivity map on the equatorial plane, as a function of time and minor radius, $\epsilon(r, \theta = 0; t)$. The solid white line indicates radial shift of the dominant mode.

The phase relationship between the toroidal positions of H_α maxima and those of the $\Delta_{1,-7}$ shift is studied on a statistical basis by computing the probability distribution function (PDF) of these maxima as a function of the magnetic shift $\Delta_{1,-7}$ and of its toroidal derivative $\frac{\partial\Delta_{1,-7}}{\partial\phi}$. As shown in figure 3 this PDF reveals that H_α maxima occur more frequently for outward shifts and negative values of $\frac{\partial\Delta_{1,-7}}{\partial\phi}$. This is equivalent to a phase shift in the range $[0, \frac{1}{4}]$ of the dominant mode toroidal wavelength. The same periodicity is confirmed by measurement of the total radiation $P_{\rm rad}$, obtained from a tomographic reconstruction [20] (see figure 4): indeed the total radiation emissivity map on the equatorial plane, as a function of time $\epsilon(r, \theta = 0; t)$, is found to be modulated by the $\Delta_{1,-7}$ shift, with higher values occurring when the $\Delta_{1,-7}$ shift points outwards.

Quantitatively the difference in the particle influx between positive and negative values of horizontal shift is shown in figure 5 where $\Gamma^{\rm in}_{H_\alpha}$ is shown as a function of $\Delta_{1,-7}$ for a set of discharges at 1.5 MA and $\langle n_e\rangle \approx 3\times10^{19}\,{\rm m}^{-3}$. Particle influx increases by a factor of 4 from 2.5 up to $9\times10^{21}\,{\rm m}^2\,{\rm s}^{-1}$ from negative to positive values of $\Delta_{1,-7}$.

An effective technique to mitigate PWI has been proved to be Li-conditioning, realized in RFX-mod through Li-pellet injection [21]. Indeed conditioned discharges exhibit a lower particle influx, and a smaller discrepancy between

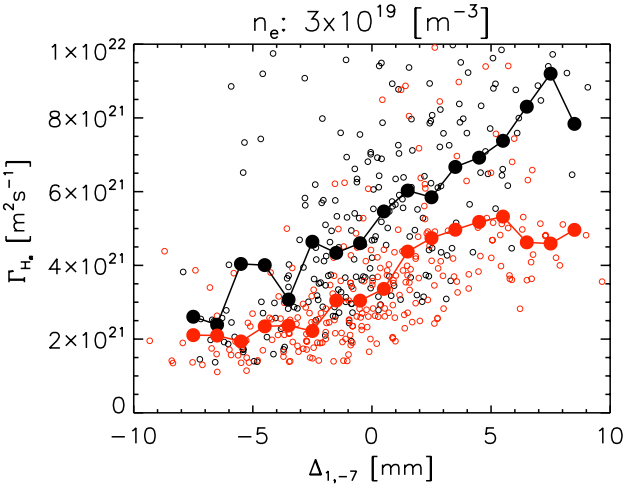

Figure 5. Particle influx estimated from H_α signal as a function of $\Delta_{1,-7}$ in normal discharges (black symbol) and lithized discharges (red symbols). Full symbols are averaged over different $\Delta_{1,-7}$ values.

regions with positive and negative plasma shifts, $\Gamma^{\rm in}_{H_\alpha}$ varying from approximately 2 up to $5\times10^{21}\,{\rm m}^2\,{\rm s}^{-1}$. This behaviour highlights the beneficial effects of Li-conditioning in decoupling magnetic topology and particle recycling: this task is indeed recognized as a key ingredient in many density limit phenomena [22].

The interest in the relationship between magnetic topology and particle sources and sinks is intertwined with two open issues in the RFP research: first the mechanism of QSH–MH back transition, which is found to occur contemporaneously to the appearance of reconnection events, and to be influenced by local density accumulation and corresponding plasma cooling. Second, the presence of a critical density limiting the operational space where QSH states can develop. Both topics will be expounded in the following sections.

2.2. *Magnetic structure and electron pressure*

The advected plasma quantities, such as density and temperature, exhibit a strong dependence on magnetic topology. The time evolution of the boundary radial profiles of electron density and temperature is measured, on the equatorial plane, by the thermal helium beam (THB) diagnostic [23, 24]. The measured radial profile spans over 30 mm from the wall (from $r/a = 0.93$ to 0.99), with a time resolution of 3 ms. This diagnostic technique is based on the intensity ratio of He I emission lines, estimated from a local He puffing in H discharges. It has already been reported [24] that the time evolutions of both electron density and temperature are strongly correlated with the local horizontal shift $\Delta_{1,-7}$, with density exhibiting an increase of about (1–2) $\times\ 10^{19}\,{\rm m}^{-3}$, corresponding to about 100%, for positive values of $\Delta_{1,-7}$ with respect to negative ones, whereas temperature exhibits a modest decrease of about 20% still for $\Delta_{1,-7} > 0$. As already observed for H_α electron pressure also exhibits a strong dependence both on the local plasma shift, as a consequence of the described behaviour of electron density and temperature, and on the toroidal derivative of this shift $\partial\Delta_{1,-7}/\partial\phi$. Furthermore, in order to discriminate a possible

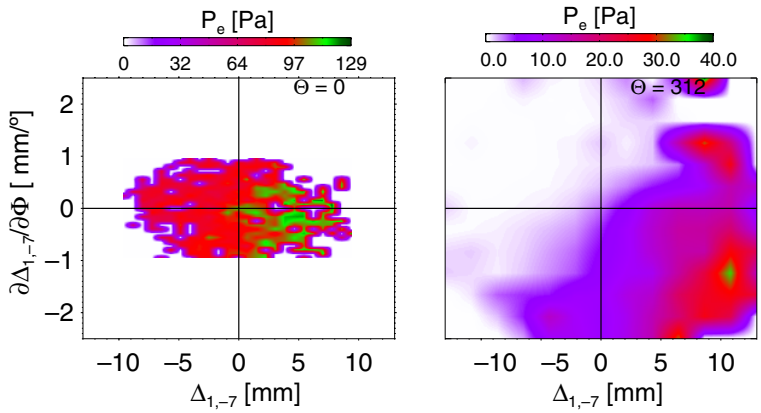

Figure 6. Electron pressure as a function of $\Delta_{1,-7}$ and $\partial\Delta_{1,-7}/\partial\phi$ as measured from THB (left panel at $\theta = 0^\circ$) and from a fixed Langmuir probe (right panel at $\theta = 312^\circ$).

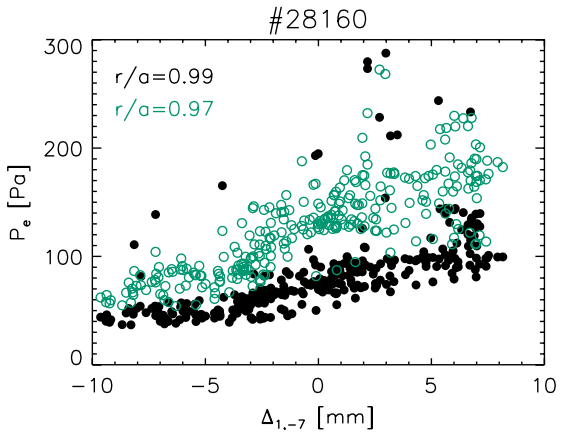

Figure 7. Electron pressure as a function of $\Delta_{1,-7}$ at two different radial positions.

poloidal dependence of this behaviour, induced by a different phase relation between $(0, 7)$ and $(1, -7)$ modes, electron pressure is evaluated by a fixed triple Langmuir probe, which provides electron density and temperature at $r/a = 1$ at $\theta = 312^\circ$ (in the bottom part of the vacuum chamber). The value of pressure as a function of $\Delta_{1,-7}$ and $\partial\Delta_{1,-7}/\partial\phi$ computed at the corresponding poloidal angle is shown in figure 6 for the two diagnostics. In both cases higher values of electron pressure are measured for positive values of $\Delta_{1,-7}$ and negative values of $\partial\Delta_{1,-7}/\partial\phi$, although the Langmuir probe exhibits a pressure variation at more extreme values of both $\Delta_{1,-7}$ and $\partial\Delta_{1,-7}/\partial\phi$. We explain this behaviour with the different radial positions of the measurements: THB data are taken at $r/a \simeq 0.97$, whereas the Langmuir probe stays at $r/a = 1$, and this requires a more extruding plasma shift to measure a pressure variation. It has to be pointed out that the behaviour of electron pressure is determined essentially by the electron density dynamics rather than temperature fluctuations, as already reported [24]. Further confirmation of the dependence of electron density on the $m = 1$ shift is provided by a single wavelength ultra-fast reflectometer, which shows that the distance of the cut-off layer density is found to oscillate in phase with the local $\Delta_{1,-7}$ [25].

Figure 7 shows the electron pressure as measured by the THB in two different radial positions ($r/a = 0.97$ and 0.99), chosen over the five available. On the x-axis we plot the shift $\Delta_{1,-7}$. In both positions pressure increases as a function of $\Delta_{1,-7}$ and, in particular, for positive values of $\Delta_{1,-7}$, which is a signature of increased PWI. The resulting edge pressure gradient is larger at $\Delta_{1,-7} > 0$ since the density profile in the edge peaks on the bulge of the helix.

2.3. *Magnetic structure and floating potential*

RFX-mod is equipped with a full set of floating potential V_f measurements pertaining to the ISIS system [26], lodged in the graphite tiles distributed in a full toroidal array plus a full poloidal array at given poloidal and toroidal positions, respectively. These measurements allow the spatial characterization of the floating potential pattern and the comparison with the helical ripple at the edge as shown in figure 8. The $n = 7$ modulation in the floating potential can be easily recognized considering panel (a) of figure 8 where V_f is shown as a function of time and toroidal angle: this $n = 7$ modulation can be linked to the helical deformation of the plasma column described by the $\Delta_{1,-7}$ shift, shown in figure 8(b) as estimated at the poloidal angle of the floating potential toroidal array. The $m = 1$ modulation can be easily observed by looking at figure 8(c) where, at a fixed toroidal position, measurements of V_f are shown as a function of time and poloidal angle. For comparison the poloidal modulation of $\Delta_{1,-7}$ is shown in panel (d). The stronger negative values of V_f fluctuations correspond to outward shift, so that the increased PWI due to the $m = 1$ shift produces a local increase in negative V_f. Such negative values are compatible with the hypothesis that electrostatic probes mounted at the wall explore a more internal plasma region [9] for positive values of $\Delta_{1,-7}$. This picture contributes to show the possible link at the edge of QSH states between magnetic modes and kinetic effects: indeed lower negative values of floating potential can be interpreted as an enhancement of electron fluxes collected by the probe.

To study the space relation of the floating potential with respect to the local magnetic topology the same analysis proposed for pressure is performed. In figure 9 two contour plots of V_f as a function of $\Delta_{1,-7}$ and $\partial\Delta_{1,-7}/\partial\phi$ are shown, comparing two different poloidal positions, one close to the equatorial plane at $\theta = 340^\circ$, and the other one close to the bottom of the vessel at $\theta = 312^\circ$. It is interesting to note that

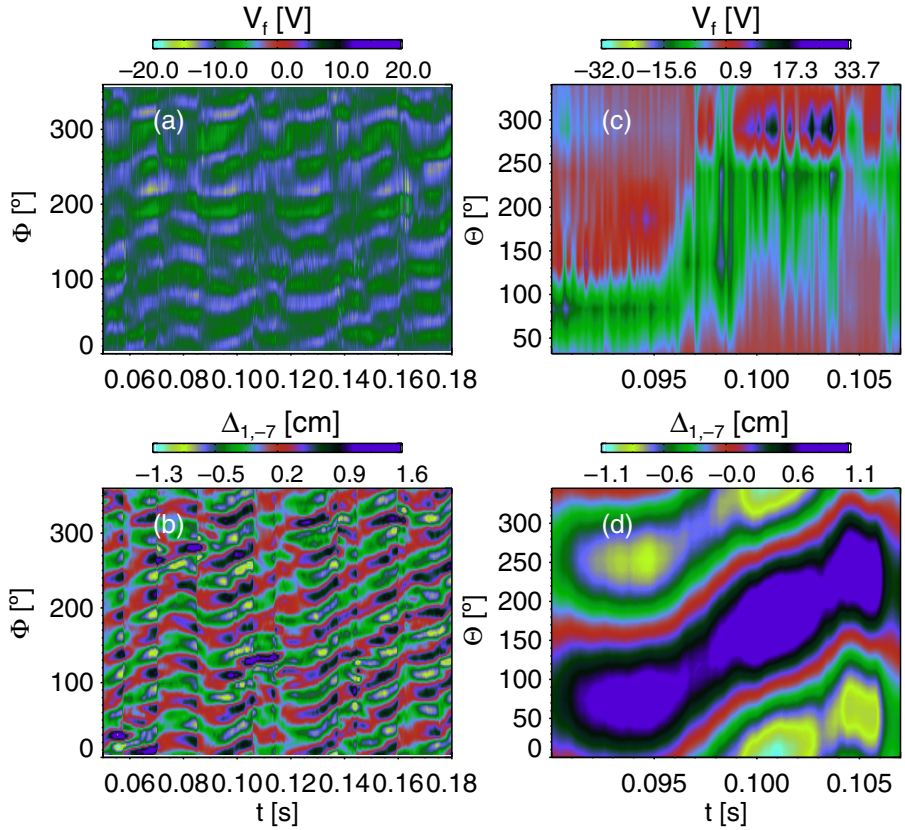

Figure 8. (*a*) Floating potential as a function of toroidal angle and time as measured at $\theta = 340^\circ$. (*b*) $\Delta_{1,-7}$ as a function of toroidal angle and time estimated at $\theta = 340^\circ$. (*c*) Floating potential as a function of poloidal angle and time estimated at $\phi = 247^\circ$. (*d*) $\Delta_{1,-7}$ as a function of poloidal angle and time estimated at $\phi = 247^\circ$.

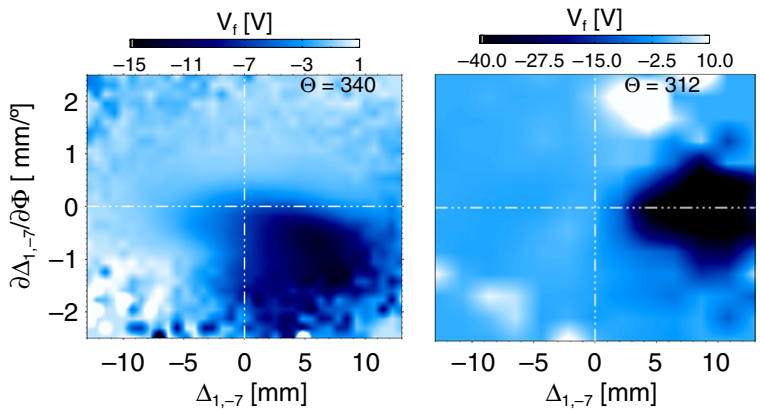

Figure 9. Floating potential as a function of $\Delta_{1,-7}$ and $\partial\Delta_{1,-7}/\partial\phi$ measured at $\theta = 340^\circ$ (left panel) and at $\theta = 312^\circ$ (right panel).

in both positions negative values of V_f are reached for positive values of the shift, but at different values of $\partial\Delta_{1,-7}/\partial\phi$. Indeed, in the lower part of the vessel, negative values of V_f are reached around $\partial\Delta_{1,-7}/\partial\phi \approx 0$: this means that V_f does not have a pure $m = 1$ dependence, since in this case the same values of V_f should be found for the same values of $\partial\Delta_{1,-7}/\partial\phi$.

2.4. Magnetic structure and flow

The flow in the boundary of RFX-mod is evaluated using different diagnostics: first of all a Gundestrup probe (in the extreme periphery) which supplies both the toroidal $M_\perp$ and poloidal $M_\parallel$ components of the Mach number close to the wall [27, 28]. In the QSH states the edge flow presents a modulation with the local shift $\Delta_{1,-7}$ on both $M_\perp$ and $M_\parallel$. A typical time behaviour of parallel Mach number in the QSH state at $r = a$ is shown in figure 10 (top panel) together with the time evolution of the local magnetic shift: around the maximum value of the shift an abrupt variation occurs with a change in the sign of the parallel flow. This behaviour is interpreted in the framework of a helical flow associated with the dominant mode and of the consequent time-dependent proximity of the $(1, -7)$ O-point to the position of the diagnostic (maximum $\Delta_{1,-7}$ corresponds to the $(1, -7)$ O-point) [27]. The positive edge parallel flow measured by the Gundestrup probes is in the direction of the

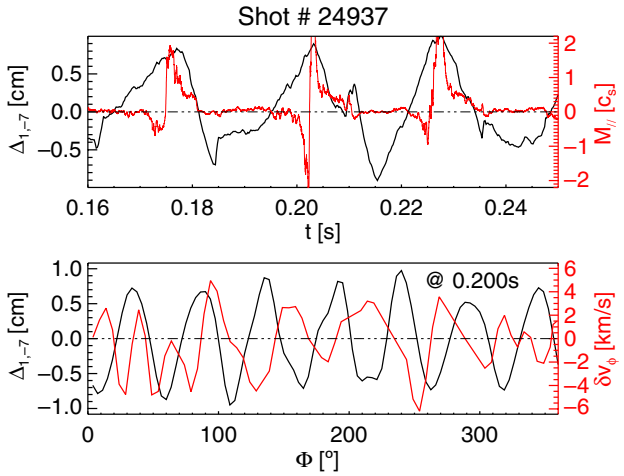

Figure 10. Top: parallel Mach number $M_{\|}$ measured at $r/a = 1$ (black line) and dominant mode radial shift $\Delta_{1,-7}$ (red). Bottom: toroidal component of velocity fluctuations as estimated from the ISIS system as a function of toroidal angle for a fixed time (black lined) compared with the values of $\Delta_{1,-7}$ (red).

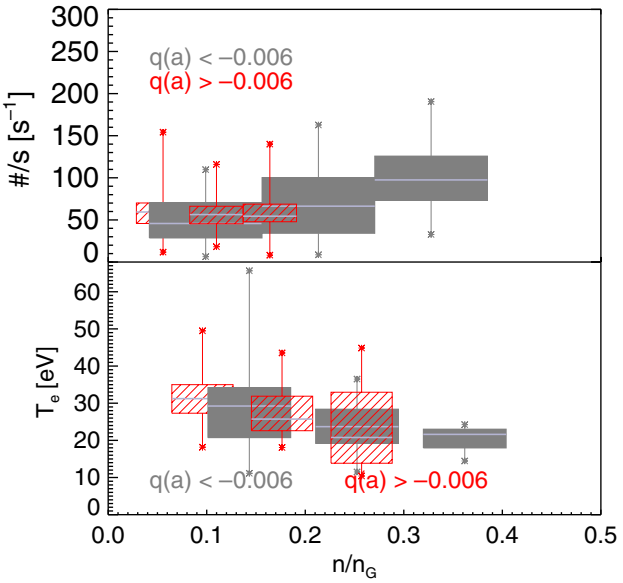

Figure 11. Top: frequency of crash events during the flat-top phase as a function of normalized density fraction. Boxes includes 50% of the distribution within the 25 and 75 percentile, horizontal lines indicate the median vertical line the minimum and the maximum values. Bottom: edge temperature as a function of n_e/n_G measured with a Langmuir probe at $r = a$.

edge poloidal magnetic field. The change in sign of the edge parallel flow, at the maximum value of the local shifts $\Delta_{1,-7}$, is in accordance with spectroscopic measurements [29] which suggests the existence of a radially directed component of the flow pointing towards the O-point of the $(1, -7)$ island. The idea that the edge flow is linked to the dominant mode $m = 1$ is corroborated by the spatial information obtained through the ISIS system using the wavelet time delay technique [30]. The toroidal component of the velocity fluctuation (at $r = a$) is shown as a function of the toroidal angle for a fixed time in figure 10, bottom panel. The fluctuations of the flow exhibit a toroidal ripple whose minima are well correlated with the maximum values of the plasma shift. The same information is also obtained through the GPI diagnostic, which gives an average value of the flow in the last 25 mm of the plasma close to the wall [27, 31]. Since the toroidal flow is linked to the radial component of the electric field through $v_\phi = E_r/B_\theta$, this experimental result means that E_r in the edge also has a toroidal ripple with seven bumps. The same toroidal dependence of E_r is seen in simulations of the ambipolar radial electric field required for balancing the electron and ion fluxes in a sheath close to the wall [15]. All these facts also support the idea of a helical flow surrounding the magnetic island $(1, -7)$ [8]: the role of this flow in the sustainment of QSH states [8] and in screening the core from impurities [32] is under investigation.

3. Dynamic of QSH crashes

At high currents the QSH states are transiently perturbed by bursts of MHD activity, which currently limit the QSH duration and deteriorate the confinement [33]. These events are partial crashes of the helical states coupled to impulsive magnetic reconnections. Measurements at low currents show that these crashes are accompanied by the formation of poloidal current sheets moving in the toroidal direction [34]. The maximum duration of QSH states (≈50 ms) is obtained at currents larger than 1.5 MA with magnetic equilibria characterized by a very shallow reversal ($q(a) \sim -0.005$) and a low Greenwald fraction ($n_e/n_G \sim 0.15$). The crash frequency is computed as the number of crashes per second occurring during the flat-top phase of the discharge. In figure 11 this frequency is shown as a function of the normalized plasma density n_e/n_G, distinguishing two different equilibria. The higher normalized density is sustainable at a relatively low value of $q(a)$ and within this equilibrium an increase in the crash frequency with n_e/n_G is observed. At more shallow $q(a)$ the operational space is limited at lower values of n_e/n_G without any clear trend. This tendency confirms the results obtained at lower currents in MH discharges in RFX-mod [34] with an increase in frequency and intensity of the crashes at deeper $q(a)$ values. In [34], the value of $q(a)$ is interpreted in terms of the ratio between reconnecting and guiding magnetic fields, since $|B_\phi(a)|/B_\theta(a) = R/a \times |q(a)|$. In this way, deeper $q(a)$ means a higher value of the ratio $|B_\phi(a)|/B_\theta(a)$. The increase in amplitude and frequency of crashes at deep $q(a)$ was obtained in the past in numerical simulations [11] and in the Los Alamos ZT-40 experiment [35]. It has already been reported that [23] edge temperature reveals a decreasing trend with normalized density fraction and this tendency is shown in figure 11 with data obtained with the aforementioned fixed edge Langmuir probe. This behaviour highlights the role of the edge temperature in the process which limits QSH duration, with an increasing rate of QSH crashes at the cooler plasma edge (with the caveat that edge temperature and density are anti-correlated, so their respective role in the reconnection process and the reason for their correlation are still under study).

A detailed investigation performed in low-current discharges [34] revealed that reconnecting events manifest with the appearance of toroidally localized, poloidal current sheets which after their formation move in the toroidal direction as an effect of $\boldsymbol{J} \times \boldsymbol{B}$ force. Current sheets in low-current plasmas are

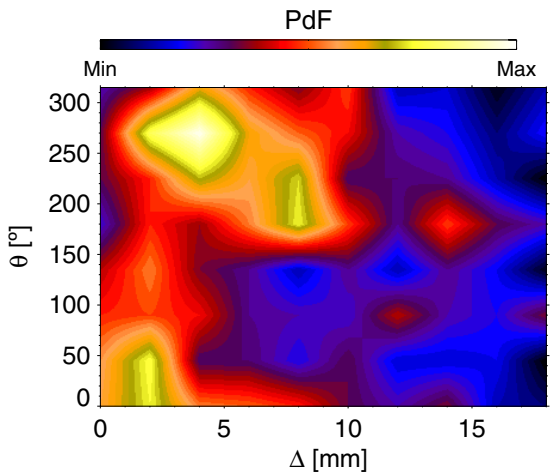

Figure 12. 2D PDF of the poloidal position of the maximum $\Delta_{1,-7}$ computed at the toroidal location where MHD crash events are observed to form.

observed to appear at the location of the wall locking, i.e. at the location of maximum PWI interaction. In high-current regimes, as reported in the previous section, wall interaction is helically distributed but experimental data confirm that MHD crash events still appear in a localized toroidal region [36]. In order to evaluate the possible influence of the (0, 7) islands in crash occurrence, we have determined the poloidal position of the maximum $\Delta_{1,-7}$ computed at the toroidal location where these events are observed to develop. The analysis is motivated by the assumption that these MHD events in high-current helical discharges take place at the location of maximum PWI, in analogy with what was observed in MH. The PDF of these data as a function of $\Delta_{1,-7}$ and θ is shown in figure 12. Most of the crashes are observed whenever the maximum value of $\Delta_{1,-7}$ is at $\theta = 250°$, i.e. at the bottom of the plasma. Due to the phase relationship between (0,7) and $(1, -7)$ modes, this poloidal position corresponds to the location where the maximum of $\Delta_{1,-7}$ (and of the local maximum of electron density) coincides with the location of the X-point of the (0,7) islands, as shown in figure 1(*b*). It is worth noting that the value of $\Delta_{1,-7}$ found is not the largest observed, but it is important that the PWI driven by $\Delta_{1,-7}$ coincides with the X-point of the (0,7) island (maximum $L_\parallel$ over ϕ at a given θ), i.e. source and accumulation point coincide. In fact, in the present first wall design, characterized by a full covering of graphite tiles [37], the main source of particles is represented by recycling with its helically shaped footprint at the maximum of $\Delta_{1,-7}$. This helical source crosses the X-points of the $(0, 7)$ islands at $\theta \approx 270°$. This means that the QSH persistence depends on the balance between particle source and accumulation at $\theta \sim 270°$, which in turn depends also on the PWI and wall conditioning.

Summarizing the analyses presented in sections 2 and 3, two poloidal positions in the machine stand out as remarkable: bottom ($\theta = 270°$) and top ($\theta = 90°$). At the bottom, the coupling of $m = 1$ O-points (particle source) and $m = 0$ X-points (particle accumulation) occurs, at the top, the coupling of both $m = 0$ and $m = 1$ X-points (larger value of $L_\parallel$) and O-points (smaller value of $L_\parallel$). This observation can be useful for future discussions on particle refuelling and/or advanced wall concepts for the RFP, such as the helical divertor [9] or the pumped limiter [38].

4. QSH persistency and density limit

At present, QSH operational space is limited in the attainable density at a relatively low value of n_e/n_G, without detectable QSH for $n_e/n_G \gtrsim 0.4$. This limit is found to depend on the amplitude of $m = 0$ modes, which in turn depends on the value of $q(a)$: it is worth remembering that $q(a)$ also determines the distance of the reversal surface from the first wall [19]. The QSH with the highest normalized density $n_e/n_G \approx 0.3$–0.4 has been obtained, up to now, at current levels of the order of 0.8 MA and safety factor $q(a) \approx -0.015$, whereas purer QSH states with longer duration and higher electron temperature are obtained at a higher current $I_p \gtrsim 1.2$ MA and a very shallow reversal ($q(a) \approx -0.005$) with a typical value of $n_e/n_G \approx 0.1$–0.2. With this equilibrium and current, higher density is reachable only transiently through pellet injection [39], or through a peculiar puffing sequence. Higher densities are also attained at $I_p \gtrsim 1.2$ MA with a feedback control of the reversal parameter $F = B_\phi(a)/\langle B_\phi \rangle$ ($\langle B_\phi \rangle$ is the toroidal field averaged on the poloidal section). This feedback control corresponds, on the other hand, to an increase in the ohmic input power up to 40–50 MW, which is likely to counteract the increased PWI found at higher densities [40].

It has already been shown [15] that within a given equilibrium, the increase in the normalized density fraction n_e/n_G determines the increase in the amplitude of the $m = 0$ modes resonating at the reversal surface, with a corresponding increase in the $m = 0$ island width. Consequently, for a given value of the reversal parameter, by increasing the normalized density $m = 0$ islands may overlap the first wall and modify the PWI. Actually, PWI in RFX-mod also strongly depends on the graphite wall capability of absorbing gas, and two possible scenarios can be drawn. In one case, experiments are run with a fresh conditioned first wall (obtained for example with prolonged He glow discharge cleaning) and with an efficient pumping capability of the graphite tiles: under this condition $m = 0$ island X-points are able to produce a divertor-like magnetic configuration, as explained in [9]. This represents the preferred operation mode of the high-current, low-density discharges. With a decrease in the pumping capability of the graphite wall, a different scenario appears: in this case, $m = 0$ islands overlap the first wall and produce an increase in the particle influx. It is worth underlining the fact that the mode frequency in RFX-mod is limited to 25–50 Hz, and the characteristic rise time of electron density (fundamentally due wall de-gassing only) is around 40–60 Hz. The rise time is calculated from the log-derivative of the density signal. In this way, the recycling pattern is always parent to the magnetic topology: this means that the neutral influxes released from the wall are not averaged over many mode periods and present a similar spatial modulation [22]. In this way, we can exploit the positive aspects of the (0,7) islands (namely, a divertor-like geometry at shallow reversal as opposed to a limiter-like geometry at deep reversal [9]) when the first wall has a good pumping capability, which currently lasts only a few discharges after conditioning.

A concise parameter used to describe this phenomenology is the Chirikov-wall parameter C_w, defined as the ratio between the $m = 0$ island half-radial width, $\Delta_0/2$, and the distance from the reversal surface to the wall, $C_w = \frac{\Delta_0}{2(a-r_{rev})}$. This parameter distinguishes between the case when $m = 0$ islands overlap the wall ($C_w \geqslant 1$) and the case when these islands are detached from the wall. C_w plays a role similar to the critical distance of the scrape-off layer from the inner wall, which in tokamaks characterizes the onset of the density limit [41]. The role of $m = 0$ and correspondingly of Δ_0 strongly depends on the equilibrium (i.e. on the reversal parameter). Indeed at deeper reversal, $q(a) \sim -0.015$, the parameter C_w remains below 1 up to $n_e/n_G \approx 0.4$ [15]. At shallow reversal, a decrease in the $m = 0$ amplitude and in the corresponding island width is observed. At the same time, the reversal radius approaches the wall, in a way that a competing process between island width and wall proximity takes place with C_w exceeding or not unity.

An example of the role played by C_w is shown in figure 13 where n_e/n_G is transiently perturbed up to 0.4 by a density burst likely induced by a local PWI event. During the density ramp-up, the amplitude of the dominant mode decreases, with the disappearance of the QSH state, which is later recovered when n_e/n_G goes back to the initial condition. In figure 13 ($q(a) \sim -0.002$) C_w experiences strong variations during a QSH cycle, in the range 2–5, always above unity. This means that $m = 0$ islands always overlap the wall. Moreover, during the QSH phase $C_w \sim 5$, decreasing during the MH interlude. The behaviour of C_w is confirmed by the Poincaré plots of figures 13(*d*) and (*e*): in QSH (panel (*d*)) the structure is more regular, with seven distinct islands, while in MH (panel (*e*)) the island chain is more segmented, with a prominent (0,1) contribution. In the Poincaré plots in (*d*) and (*e*) the three horizontal lines (orange, green and blue from top to bottom) correspond to the radial locations of the wall, the reversal and the $m = 0$ separatrix, respectively. $\Delta_0/2$ is the distance between the green and blue lines, $a - r_{rev}$ the distance between the green and orange ones. In this way, C_w can easily be visualized as the ratio between these two distances, the wall overlap thus being larger in QSH due to a larger $\Delta_0/2$. In this way, the loss of QSH cycles (whose periodicity is governed by local reconnections, as described in section 3) can be ascribed to the strong role played by the density increase due to wall out-gassing.

As a matter of speculation we can argue that the range of normalized density attainable at shallow $q(a)$, $0.05 \leqslant n_e/n_G \leqslant 0.3$, is determined by different competitors, namely $m = 0$ island width, wall proximity to the reversal surface and wall conditioning. Considering that with the increase in the plasma current both the dominant mode $(1, -7)$ [5] and its $m = 0$ counterpart (0,7) are observed to increase, this might explain the encountered difficulties in obtaining high-density, high-current regimes.

It is worth recalling that RFX-mod discharges are generally run with a pre-filling hydrogen injection, and the density is sustained throughout the discharge by the gas desorbed by the graphite wall, which represents a natural gas reservoir. The large particle influx ensured by the graphite wall essentially determines the edge density and the pressure gradient: this is observed, for example, considering the pressure characteristic scale length $L_p = -P_e/\nabla P_e$ as

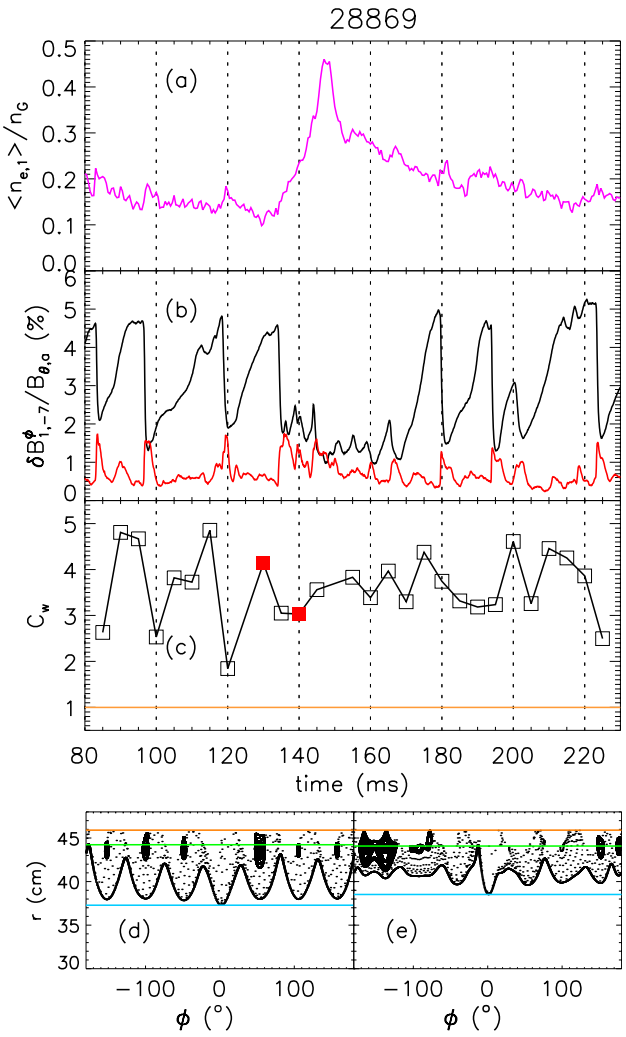

Figure 13. From top to bottom: (*a*) Greenwald density fraction, (*b*) $m = 1, n = -7$ mode amplitude (black), $m = 1, n < -7$ 'secondary' mode amplitude (red); (*c*) Chirikov wall parameter C_w; (*d*), (*e*) Poincaré plots (equatorial section at $\theta = 0$) corresponding to the solid squares in (*c*). Data refer to a discharge where n_e/n_G greater than 0.15 is transiently reached, with the QSH transiently disappearing as a consequence. QSH is recovered when n_e/n_G goes back to its initial value. Note that Chirikov parameter stays always above unity. In (*d*) and (*e*) the three horizontal lines (orange, green and blue from top to bottom) correspond to the radial locations of the wall, the reversal and the $m = 0$ separatrix, respectively.

measured by the THB, which is found to depend only on the plasma shift and to be almost independent of the plasma current, with typical values of approximately 15–25 mm. This limitation may be overcome through proper wall conditioning, which augments the hydrogen trapping capability of the graphite tiles: a technique now under investigation in RFX-mod is lithium wall conditioning [21]. As the pressure behaviour reflects the density one, Li-conditioning appears as a useful tool to create a hotter, less dense plasma in the extreme periphery which is mandatory in order to achieve better performances.

5. Conclusion

In this paper we have provided a detailed description of the boundary of a RFP plasma in the so-called quasi-single helical

(QSH) regime. In this regime the edge plasma is strongly influenced by the helical deformation (ripple) induced by the dominant mode, $\Delta_{1,-7}$. The boundary region with a positive value of $\Delta_{1,-7}$ is characterized by an enhanced PWI with a local electron pressure increase (essentially reflecting density behaviour) and more negative floating potential, even if the behaviour of the potential is more complex than a one-to-one relationship with the $m = 1, n = -7$ dominant mode. Summarizing, due to the full graphite covering of the wall [37], the main source of particles is represented by wall recycling in the shape of a helix at the maximum $\Delta_{1,-7}$, as clearly shown in the H_α signal and in the bolometric tomography.

QSH states are found to be transiently disturbed by impulsive MHD events accompanied by reconnection processes. These events are favoured when the helical source traverses the X-points of the (0, 7) islands, and this happens at the bottom of the device. This establishes a strong link between QSH persistency and local edge conditions.

The operational space for helical states in RFX-mod is found to be limited in attainable normalized density fraction. This limit depends on different competing mechanisms: $m = 0$ island width, wall proximity of the reversal surface and wall conditioning. After a few shots from wall conditioning, the PWI due to the MHD dynamics produces a wall out-gassing and a consequent loss of QSH cycles. The amelioration of the PWI in the QSH state and the widening of its operational space are therefore crucial issues for an upgrade of the RFP configuration. In this respect, an improvement of wall conditioning with lithization techniques [21] and with plasma refuelling by pellet injection are scheduled in the 2011 RFX activity programme and are envisaged to broaden the density operational space. Finally, an indication of a helical flow associated with the dominant mode is shown: further investigation will establish the role of this flow in the formation of improved confinement regimes, together with the comprehension of its role in the determination of the dynamo electric field which is essential to sustain the helical equilibrium.

Acknowledgments

This work was supported by the Euratom Communities under the contract of Association between EURATOM/ENEA. The views and opinions expressed herein do not necessarily reflect those of the European Commission. The authors would like to thank all the technical staff of RFX-mod and particularly Mr Vannino Cervaro for his work on the thermal helium beam diagnostic. One of the authors (GS) would like to dedicate this work to the birth of his son Walter.

References

[1] Paccagnella R. *et al* 2006 *Phys. Rev. Lett.* **97** 075001
[2] Ortolani S. and the RFX team 2006 *Plasma Phys. Control. Fusion* **48** B371
[3] Zanca P., Marrelli L., Manduchi G. and Marchiori G. 2007 *Nucl. Fusion* **47** 1425
[4] Marrelli L. *et al* 2007 *Plasma Phys. Control. Fusion* **49** B359–69
[5] Lorenzini R. *et al* 2009 *Nature Phys.* **5** 570–754
[6] Puiatti M. *et al* 2009 *Plasma Phys. Control. Fusion* **51** 124031
[7] Valisa M. *et al* 2008 *Plasma Phys. Control. Fusion* **50** 124031
[8] Cappello S., Bonfiglio D. and Escande D.F. 2006 *Phys. Plasmas* **13** 056102
[9] Martines E., Lorenzini R., Momo B., Munaretto S., Innocente P. and Spolaore M. 2010 *Nucl. Fusion* **50** 035014
[10] Cappello S. and Biskamp D. 1996 *Nucl. Fusion* **36** 571–81
[11] Cappello S. and Biskamp D. 1996 *The 1996 Int. Conf. on Plasma Physics (ICPP 96) (Nagoya, Japan, 1996)* vol 1, ed P E Stott *et al* (Bristol: Institute of Physics Publishing) pp 854–7
[12] Terranova D. *et al* 2010 *Plasma Phys. Control. Fusion* **52** 124023
[13] Gobbin M., Spizzo G., Marrelli L. and White R.B. 2010 *Phys. Rev. Lett.* **105** 195006
[14] Spizzo G., Cappello S., Cravotta A., Escande D.F., Predebon I., Marrelli L., Martin P. and White R.B. 2006 *Phys. Rev. Lett.* **96** 025001
[15] Spizzo G. *et al* 2010 *Plasma Phys. Control. Fusion* **52** 095011
[16] White R. and Chance M. 1984 *Phys. Fluids* **27** 2455–67
[17] Zanca P. and Terranova D. 2004 *Plasma Phys. Control. Fusion* **46** 1115–41
[18] Zaslavsky G.M. 2002 *Phys. Rep.* **371** 461–580
[19] Puiatti M. *et al* 2009 *Nucl. Fusion* **49** 045012
[20] Martin P. *et al* 1997 *Rev. Sci. Instrum.* **68** 1256–60
[21] Dal Bello S. *et al* 2010 *Proc. 23rd IAEA Fusion Energy Conf. (Daejeon, Korea, 2010)* http://www-pub.iaea.org/mtcd/meetings/PDFplus/2010/cn180/cn180_papers/exd_p3-06.pdf
[22] Liang Y. *et al* 2005 *Phys. Rev. Lett.* **94** 105003
[23] Agostini M., Scarin P., Cavazzana R., Sattin F., Serianni G., Spolaore M. and Vianello N. 2009 *Plasma Phys. Control. Fusion* **51** 105003
[24] Agostini M., Scarin P., Cavazzana R., Fassina A., Alfier A. and Cervaro V. 2010 *Rev. Sci. Instrum.* **81** 10D715
[25] De Masi G., Cavazzana R., Moresco M. and Martines E. 2011 *Nucl. Fusion* **51** 053016
[26] Serianni G., Baker W. and Dal Bello S. 2003 *Rev. Sci. Instrum.* **74** 1558–62
[27] Spolaore M. *et al* 2010 *J. Nucl. Mater.* at press (doi:10.1016/j.jnucmat.2010.12.029)
[28] De Masi G. *et al* 2010 *Contrib. Plasma Phys.* **50** 824–9
[29] Bonfiglio D., Bonomo F., Piovesan P., Piron L. and Zaniol B. 2010 *Proc. 37th EPS Conf. on Plasma Physics (Dublin, Ireland, 2010)* vol 34A p O2.101 http://ocs.ciemat.es/EPS2010PAP/pdf/O2.101.pdf
[30] Jakubowski M., Fonck R., Fenzi C. and McKee G. 2001 *Rev. Sci. Instrum.* **72** 996–9
[31] Scarin P., Agostini M., Cavazzana R., Sattin F., Serianni G., Spolaore M. and Vianello N. 2009 *J. Nucl. Mater.* **390–391** 444–7
[32] Menmuir S., Carraro L., Alfier A., Bonomo F., Fassina A., Spizzo G. and Vianello N. 2010 *Plasma Phys. Control. Fusion* **52** 095001
[33] Piovesan P. *et al* 2009 *Nucl. Fusion* **49** 085036
[34] Zuin M., Vianello N., Spolaore M., Antoni V., Bolzonella T., Cavazzana R., Martines E., Serianni G. and Terranova D. 2009 *Plasma Phys. Control. Fusion* **51** 035012
[35] Watt R.G. and Nebel R.A. 1983 *Phys. Fluids* **26** 1168–70 http://link.aip.org/link/?PFL/26/1168/1
[36] Scarin P. *et al* 2010 *Proc. 23rd IAEA Fusion Energy Conf. (Daejon, Korea, 2010)* http://www-pub.iaea.org/mtcd/meetings/PDFplus/2010/cn180/cn180_papers/exd_p3-29.pdf
[37] Zaccaria P., Dal Bello S. and Marcuzzi D. 2003 *Fusion Eng. Des.* **66–68** 289–93 ISSN 0920-3796 *22nd Symp. on Fusion Technology (Helsinki, Finland, 2002)* http://www.sciencedirect.com/science/article/B6V3C-48R1XWD-J/2/a7c78ba717fd255dbbe90bfba1540876

[38] Sonato P., Antoni V., Carraro L., Puiatti M., Serianni G., Scarin P., Spolaore M., Valisa M. and Zaccaria P. 2002 *Plasma Phys. Control. Fusion* **44** 627

[39] Terranova D., Auriemma F., Canton A., Carraro L., Lorenzini R. and Innocente P. 2010 *Nucl. Fusion* **50** 035006

[40] Agostini M. 2011 *RFX-mod Programme Workshop 2011 (Padova, Italy, 2011)* http://www.igi.cnr.it/rfxmod2011/presentations/Agostini1.pdf

[41] De Vries P., Rapp J., Schüller F. and Tokar M. 1998 *Phys. Rev. Lett.* **80** 3519